Available online at www.sciencedirect.com
ScienceDirect
Physics Procedia 1 (2008) 305–313
Physics Procedia
www.elsevier.com/locate/procedia

Proceedings of the Seventh International Conference on Charged Particle Optics

CHARIOT: software tool for modeling SEM signal and e-beam lithography

S. Babin *, S. Borisov, A. Ivanchikov, I. Ruzavin

Abeam Technologies, 5286 Dunnigan Ct., Castro Valley, CA 94546, USA

Received 9 July 2008; received in revised form 9 July 2008; accepted 9 July 2008

Abstract

An advanced Monte Carlo software tool CHARIOT was developed to simulate image formation in SEM, energy deposition in EBL, electron spectra, and charging of a target. Scattering of an electron beam in a microstructure, generation of secondary electrons, and characteristics of the detector, as well as the material and shape of the features, determine electron scattering and a SEM signal. Physical and mathematical models are described to comply with an accuracy required by modern technology, especially at low voltage electrons. Examples of applications to CD-SEM, defect inspection, EBL, and electron spectrometer are presented.

PACS: 02.70.Uu; 41.85.-p; 85.40.Hp

Keywords: Monte Carlo; Software; Electron Beam; Energy deposition; Charging; Secondary electrons

1. Introduction

Monte Carlo methods to simulate electron scattering in solids were extensively developed in the 1960s [1-5]. Modern technology has recently given rise to a new round of interest in Monte Carlo simulators, at a new level of accuracy. Demanding requirements on the performance of electron beam lithography (EBL), scanning electron microscopy (SEM), and especially CD-SEM require understanding and prediction of electron-to-target interactions. Because of the complexity of the physics involved in electron scattering, understanding and accurate extraction of a SEM signal formation mechanism and absorbed energy in EBL are problematic. To respond to this problem, CHARIOT software employs advanced physical models to satisfy the required accuracy.

Monte Carlo simulators often involve continuous slowing down approximations (CSDA) for inelastic energy loss and the Rutherford formula for elastic scattering. Electron energy losses are described by the average energy continuously released along the trajectory, usually using the Bethe-Bloh formula. These models give good estimations but cannot be used for a detailed analysis, especially at low voltages. As opposed to CSDA, a discrete loss approximation (DLA) considers all scattering events separately, without averaging. It tracks elastic scattering,

* Coresponding author. Tel: +1-510-415-6032
E-mail address: sb@abeamtech.com

doi:10.1016/j.phpro.2008.07.110

ionization of inner and outer atomic shells, excitation of plasmons, etc., emulating individual events along the electron trajectory.

In this paper, physical models and a software program are described. Examples of simulations are presented for defect inspection, electron beam lithography, CD-SEM, and electron spectrometer. The simulations were done using both CSDA and DLA models; much better accuracy of the DLA model used in CHARIOT was demonstrated.

2. Physical models

CHARIOT software considers elastic electron scattering using either the Mott or Rutherford model, inelastic energy loss using the Bethe [7] formula, or generation of fast and true secondary electrons using the Gryzinski [8] and Moeler [9] model for atomic inner and outer shells, respectively, together with plasmon mechanisms, and electron propagation between layers.

In addition to the scattering model, the software considers accumulation and dissipation of charge, trajectories of electrons in an electrical field, specifics of electron beams, and also detector geometry, location, and its energy transfer function.

2.1. Electron scattering: discrete energy loss

For the computation of an inner-shell ionization cross-section, the Gryzinsky formula was used:

$$ds(E') = \frac{pe^4}{EE_s^2}\left[\frac{E}{E+E_j}\right]^{3/2}\left[1-\frac{E_s}{E}\right]^{E_j/(E+E_j)}\left[1-\frac{E_j}{E}+\frac{4E_j}{3E_s}ln\left[2.7+\sqrt{\frac{E-E_s}{E_j}}\right]\right] \quad (1)$$

where E is primary electron energy, E_j is $j^{\text{-th}}$ electron binding energy.

The excitation cross-section of volume plasmons can be defined by the model developed in [10].

$$s_{pl}(E) = \frac{n_n pe^4}{EE_p} ln\left[\frac{J_C^2+J_E^2}{J_E^2}\right], \text{ where } J_E = \frac{E_p}{2E}, J_c = 0.353\sqrt{\frac{E_f R_0}{Ea_0}}, E_p = \hbar\sqrt{\frac{4pN_a e^2}{m}} \quad (2)$$

Here n_n is an averaged number of valence electrons, J_C is the critical deflection angle of primary particle, up to which the collective oscillation of electron plasma can be excited; $E_p$is a plasmon energy, which is evaluated using Lengmure's formula; R_0 is the averaged distance between free electrons; E_f is the Fermie energy, a_0 is the first Bore radii; m is electron mass; h is the Plank constant; N_n is the volume concentration of free electrons, $N_n = rN_a n_n/A$.

At the scattering angle $q > J_C$ the interaction with valence electrons becomes a single-particle interaction rather than a collective one. In this case, a Moeler crossection is used, with addition of the so-called interchange member due to quantum effects. This cross-section per atom is the following:

$$\frac{ds(q)}{de} = n_n\frac{pe^4}{E^2}\left[\frac{1}{e^2}+\frac{1}{(1-e)^2}-\frac{1}{e(1-e)}\right] \rightarrow e_c < e < \frac{1}{2} \quad (3)$$

Where $e_c = \sin^2 J_c$

The simulation of the electron trajectory using cross-sections described above holds down to the threshold energy E_c. Energies below the threshold electron penetration are described by another model or considered to be stopped. In the present work, the threshold value of E_c = 0.1 keV was determined to be an optimum threshold value for the models used.

Energy losses caused by all other interaction processes, such as electron–photon interaction, surface plasmon excitation, etc., were estimated to be smaller then 5% of total losses and can be neglected.

Detailed simulation of slow (a few tenths eV) electron scattering requires significant computation time. In some cases, for example for metals and some semiconductors, the semi-empirical scattering model can be constructed. Let us assume the scattering of slow (with energies <100 eV) electrons to be isotropic by the scattering angle [11]. So the energy of the primary and secondary electrons can be defined as, $E'=\sqrt{\xi}$, $E''=(1-\sqrt{\xi})$, where ξ is a random value uniformly distributed within the segment [0,1].

Mean free path between these interactions for elements (λ_1) and for the inorganic compounds (λ_2) can be found using formulas [12, 13]:

$$\lambda_1(E) = a\left\{\frac{538}{(E-E_F)^2}\right\} + 0.41a\sqrt{(E-E_F)}, \quad \lambda_2(E) = a\left\{\frac{2170}{(E-E_F)^2}\right\} + 0.72a\sqrt{(E-E_F)} \tag{4}$$

Here λ is the free length between the interactions in nm, $a^3=A/\rho n N_A \cdot 10^{24}$ (nm^3), where a is the thickness of monomolecular layer in nm. For the organic compounds, λ in mg/m is equal to

$$\lambda(E) = \frac{49}{(E-E_F)^2} + 0.11\sqrt{(E-E_F)} \tag{5}$$

It is also assumed that each non-escaped electron collides non-elastically[14]. For the surface potential barrier, a model was introduced to take into consideration the surface effect. The maximum angle α, at which electrons can penetrate this barrier, is defined by the normal component of the electron impact $\sqrt{2m(E_f+\varphi)}$. Here φ is the work function of material.

2.2. Electrical fields

An influence of electrical fields on electron trajectories is considered. The electrical field can be defined

- By using data of E-field, for example, a file resulting from simulations using MEBS software
- By the potential between a sample and a detector or any other plane
- As the result of charging a sample with an electron beam

Electron trajectories of both primary and secondary electrons are subject to the influence of the electrical field. It is known that trajectories become curved in the presence of the field. Deflection of primary electrons from the intended target point may lead to beam placement errors. Change in trajectories of backscattered electrons results in variation of the number of electrons that reach a detector and, therefore, variation of SEM signal. These effects result in distortion of SEM image, placement errors in EBL, and significant change of electron spectra.

2.3. Charging

Electrons may produce positive or negative charging of a target, which influences electron trajectories. The deposited charge is tracked in a target separately for positive and negative values. The deposited charge is dissipated in the target. Depending on electrical properties of materials, the discharge and incoming electron beams define charge distribution in a target at any moment at and after irradiation.

The target is described in such a way that the mesh used in the discharge model covers exact boundaries of layer figures. This allowed for an accuracy needed in simulation of the discharge. The discharge model involves complex algorithms that will be described elsewhere.

3. CHARIOT software

CHARIOT software includes a simulation engine and a sophisticated graphical interface to prepare descriptions of a 3D target, beam, and electron detector. The software considers:

- Advanced Monte Carlo model of electron scattering in materials
- 2D and 3D multilayered patterns
- A variety of e-beam configurations: point, Gaussian, and rectangular shape; tilted and conical beams
- Electron trajectories in an electrostatic field
- Geometry and energy transfer function of a detector

A user-friendly graphical user interface (GUI) was developed. This powerful GUI allows a great deal of flexibility and a full range of parameters, while being intuitive and easy-to-learn. Input parameters for the software are described below.

3.1. 3D target

Each layer of a target can be specified separately, including chemical composition, physical properties, and geometry of the pattern. Layers can automatically be combined to imitate such processes as etch, film deposition, and lift-off. In this way, a complex 3D pattern like a microcircuit can be specified. A library of constants for a variety of materials is provided.

An example of setting up a target is presented. A line with a specified profile is defined, then placed as an array (see Fig. 1, a,b). An additional layer, structured as two stripes perpendicular to the lines is added; the software automatically makes a “lift-off” process to build a 3D target as shown in Fig. 1 c,d.

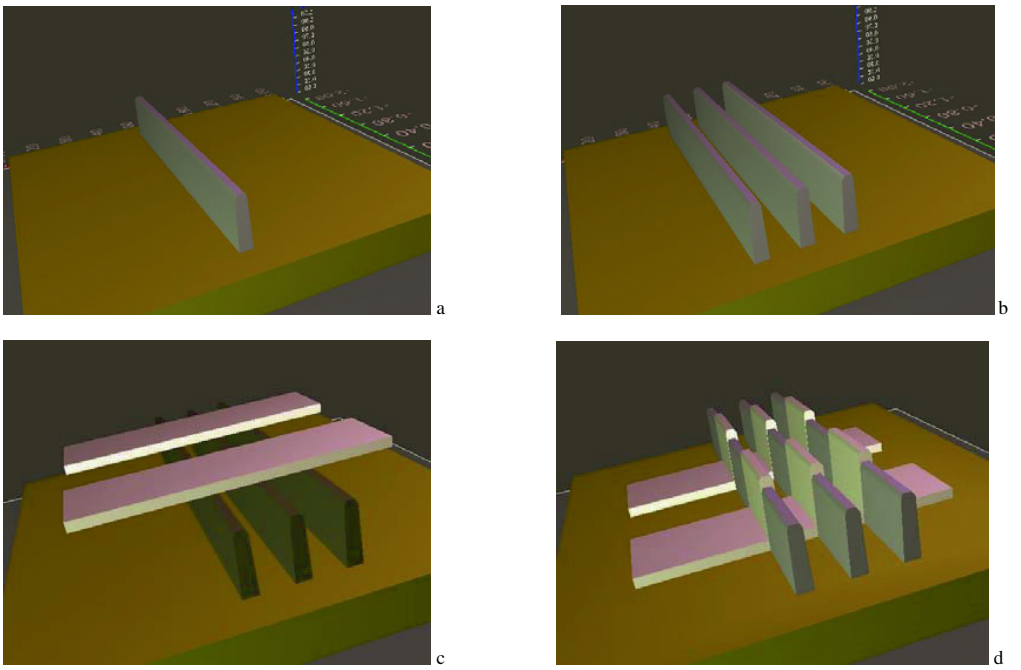

Fig. 1. A line with a specified profile (a) is multiplied in one direction (b); an additional layer structured as two stripes is added (c) and automatically built to define a 3D pattern (d)

3.2. Beams

Beam voltage, current, and size are specified. The shape of the beam can be a point, Gaussian, or a rectangle. The beam can be parallel or conical with a specific numerical aperture. The beam can also be tilted from a vertical direction.

In addition, beams can scan in one direction or two directions, see Fig. 2. The scanning may go as a raster or a meander. All timing and delays involved in scanning can be specified. In this way, the software emulates an actual irradiation order.

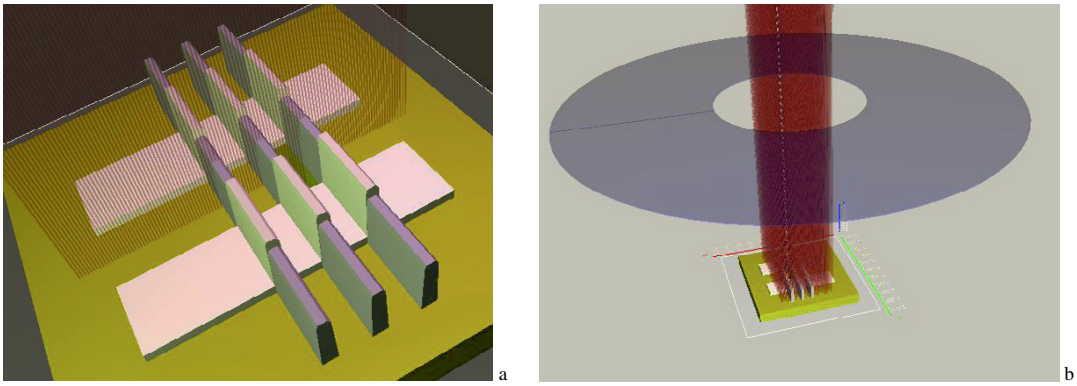

Fig. 2. (a) One dimensional scanning of a beam over the pattern;
(b) a ring-shaped backscatter detector is placed above the pattern; beam scanning is two-dimensional

3.3. Electron detector

Detection of electrons is an important part of input data. The resulting signal depends heavily on the position of the detector and its geometry. For example, a ring-shaped backscatter detector (see Fig. 2b) will produce a different signal than a detector placed to the side of the target. An energy transfer function, which is the detector signal as a function of electron energy, is also an important factor. All these parameters can be specified by the user.

3.4. Physical models

Both CSDA and DLA models are implemented in CHARIOT. Fast simulations can be done using the CSDA approach; accurate simulations use the more complex DLA model.

3.5. Cluster versions

Monte Carlo simulations are statistical; therefore, significant simulation time is required to achieve good accuracy. A typical simulation takes from one minute to tens of hours. In order to shorten simulation time, a cluster version was developed. The software works on clusters under Windows, Unix, and Mac-OS platforms.

4. Simulation results

4.1. Defect inspection

In defect inspection, it is important to know if a certain defect can be found at specific SEM settings. An example of simulation is shown in Fig. 3. The pattern is five lines of resist with specified vertical profiles on silicon. The

middle line involves a defect – a hole through the line. Electron trajectories as an intermediate result of simulation are displayed in Fig. 3b. They have been simulated in the presence of an electrical field; therefore, the trajectories are curved. A SEM signal was simulated for 2 kV electron beam and a specified in-lens detector. Depending on specific properties of the defect and electron beam, the defect can be clearly detected or can be missed, see Fig. 3, c,d.

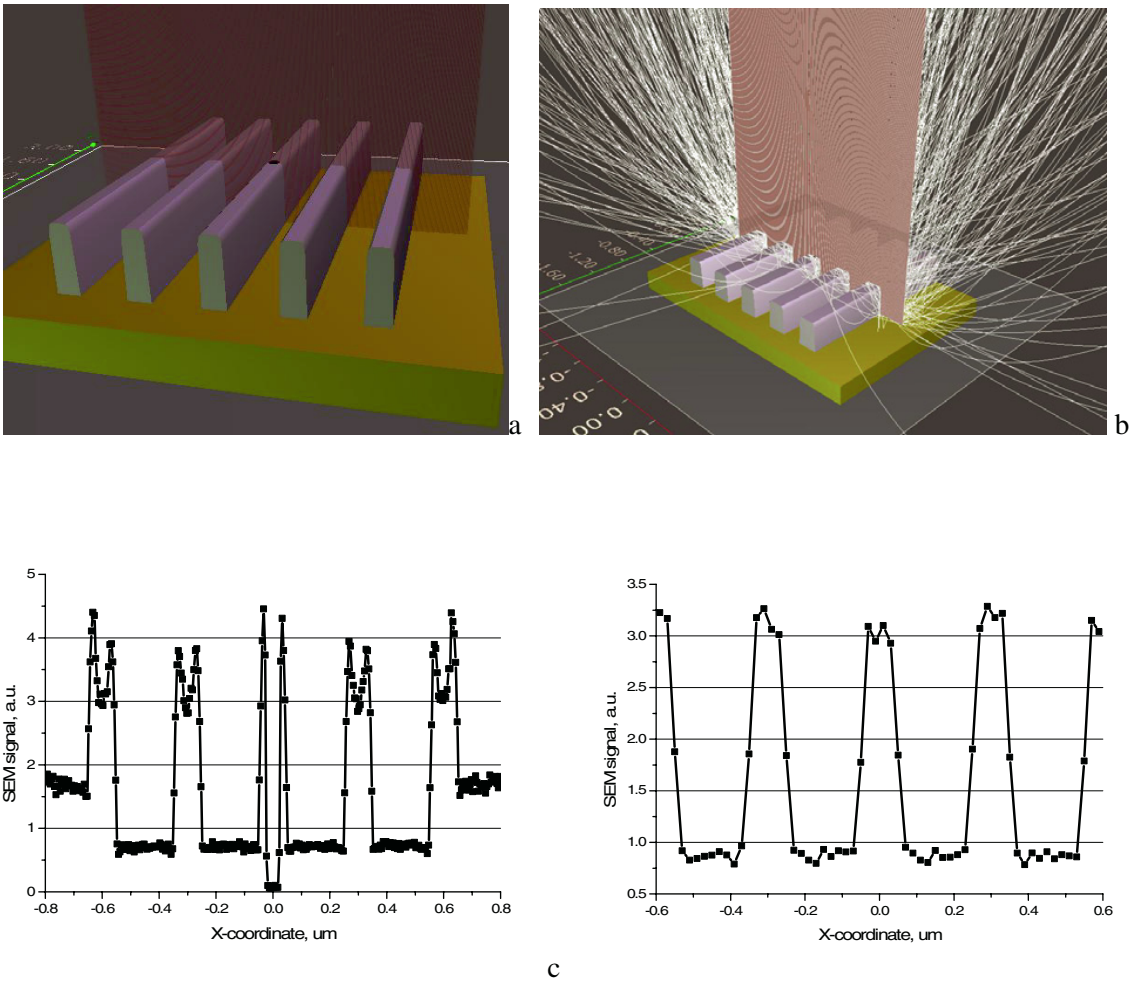

Fig. 3. Defect detection project: five profiled lines; the middle line has a defect as a hole in the center of a line (a) Trajectories of backscattered electrons are shown as an intermediate result of simulation (b). A signal from a detector: (c) the defect is clearly visible when its size is 50 nm diameter and a beam is 3 nm; (d) non-detectable when beam size is 20 nm, defect size is 10 nm

4.2. Simulation of CD-SEM

One critical task in semiconductor manufacturing is measurement of linewidths with accuracy of better than 1 nm. A cross-correlation of CD-SEMs is often subject to a significant absolute linewidth error. There is no proven algorithm for edge detection in CD-SEMs. Tool manufacturers set up the edge detection threshold voluntarily, as a rule, which is why the absolute errors in measurement occur.

We demonstrated that edge detection depends greatly on parameters of SEM settings, like beam diameter, and on pattern properties, like wall angle of a pattern (Fig. 4). In simulation, both the signal and pattern are known; therefore, an offset for a specific SEM algorithm can be found. Having this data, an algorithm for automatic edge detection in CD-SEMs can be tuned for beam parameters and the type of a pattern.

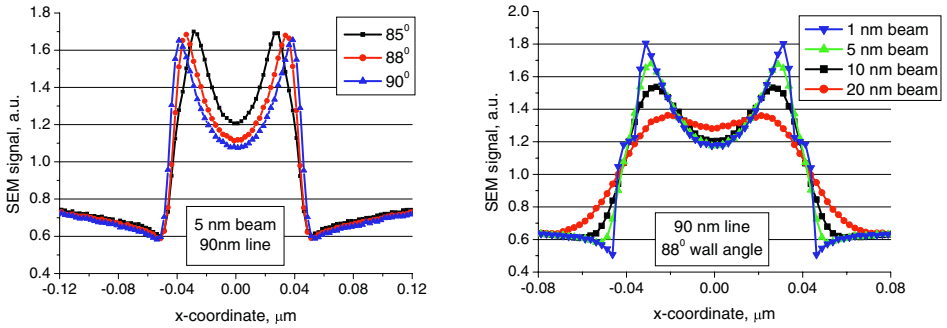

Fig. 4. SEM signal profiles of resist lines on silicon: (a) at variable wall angle, (b) at variable beam size

Simulations for various parameters of beam and a pattern proved that there is a variable parameter-specific error of linewidth measurement in addition to the offset between edge position and a peak of a signal. An error in measurement of edge position due to beam size instability was found to be up to 11 nm on top of the regular offset error when beam diameter changes from 1 nm to 20 nm [15]. Comparison of a simulated SEM signal with a pattern would allow to define the edge position and calibrate a SEM so that any system- and pattern-dependent errors can be removed.

4.3. Energy deposition in electron beam lithography

In EBL, electrons scatter in the resist and substrate, causing redistribution of absorbed electron energy and variation of critical dimensions (CD). The knowledge of this redistribution in the resist is important for accurate correction of the distortion. In both maskmaking and in direct write EBL, a multilayered, 3D target can be specified; electron scattering can be determined for specific settings of an electron beam. An example simulation result is presented in Fig. 5, where the energy spread in the resist on silicon is shown at 50 keV and 100 keV electrons. At higher voltage, the lateral beam-scattering range in the resist is considerably smaller. This is why 100 keV is often used for high-resolution lithography at a scale of a few nanometers or a few tens of nanometers.

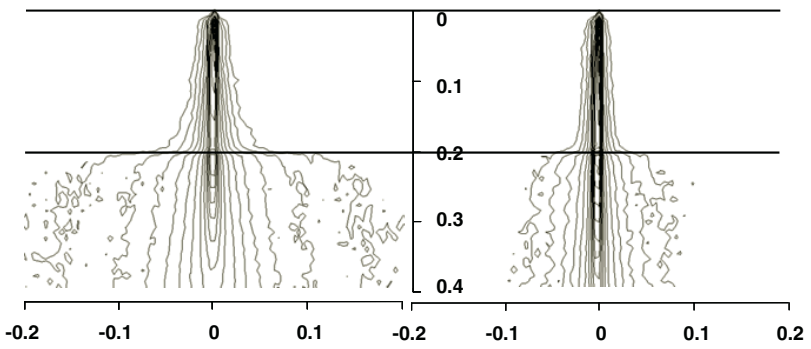

Fig. 5. Absorbed energy in 200 nm thick resist on silicon at 50 keV and at 100 keV electrons

4.4. Electron spectrometer

Electron spectra of transmitted and backscattered electrons are used for characterization of materials. A capability for accurate simulation is needed. In this section, we will demonstrate that a complex DLA model is appropriate for such simulations while other methods fail.

Spectra of transmitted electrons were simulated using CSDA and DLA models. Energy of primary electrons was 20 keV; the thickness of gold film was 43 nm. Spectra of transmitted electrons are presented in Fig. 6. The result is qualitatively different for the two models used. Experimental data from [12] showed good correspondence to results received using the DLA model and strong disagreement with the CSDA model.

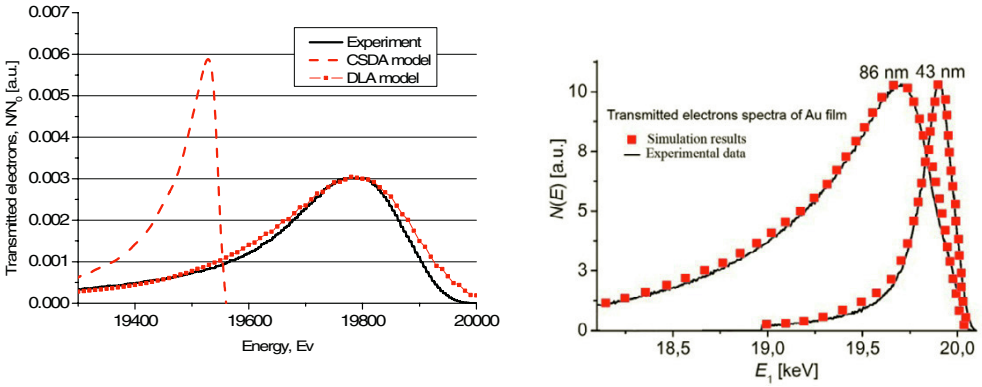

Fig. 6. (a) Comparison of the transmitted electron spectra resulting from DLA, CSDA models and the experiment [12]. (b) Transmitted electron spectra simulated using DLA model and experimental data at two thicknesses of gold films

This difference in DLA and CSDA results is understandable when we take into account the fact that energy loss in the CSDA model depends on the length of the electron trajectories. The energy loss E in transmission through a material of thickness l is a function of the thickness:

$$E = \int_0^l \frac{dE}{dx} dx \tag{6}$$

As long as the film thickness differs from zero, a certain electron energy is lost. Therefore, the CSDA model by its nature does not allow electrons with energies near those of primary electrons; a correct result is not possible.

In the DLA model, electrons lose energy in random amounts according to the differential interaction cross-sections at the points of each interaction. The simulation algorithm takes into account all significant interactions (elastic, inner and outer atomic shell ionization, etc.) separately. This is why the DLA spectra become similar to experimental data. Electron spectra at two thicknesses of gold film have been simulated and compared to experimental results, see Fig. 6b. A good correspondence was found.

Landau theory describes the loss of electron energy in transmission through thin film [6]. The formula is valid when the film thickness is much smaller than the penetration depth of electrons. Results of Landau and the DLA model are in a good agreement, see Fig. 7a. In this case, the DLA model did not consider the plasmon generation mechanism, same as the Landau model.

On the other hand, when the plasmon mechanism is turned on in the DLA model, simulation can predict details of the spectra; these are new results, which are not possible to achieve using either the Landau or the CSDA approach. When a full DLA model is used, it reveals sharp plasmon peaks in electron spectra, as shown in Fig. 7b.

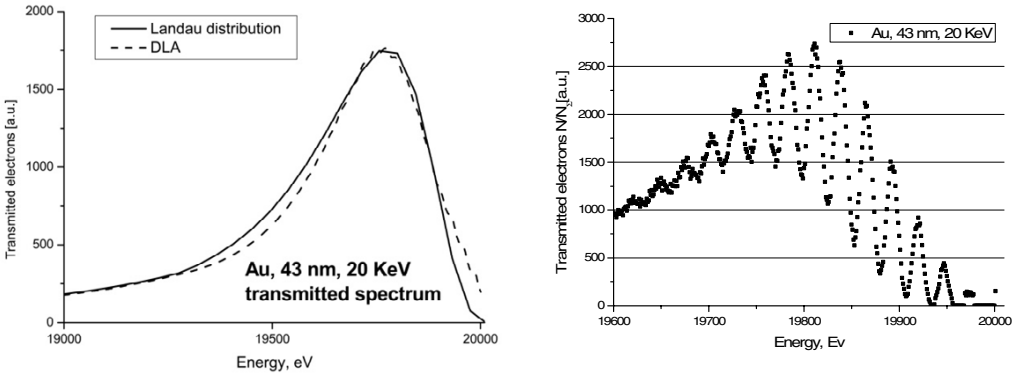

Fig. 7. (a) Transmitted spectra using the DLA and Landau models are in good agreement when the plasmon mechanism is turned off in DLA. (b) The full DLA model reveals details of electron spectra, which are not possible to achieve using either Landau or CSDA models. Sharp plasmon peaks are clearly visible

5. Conclusion

CHARIOT software was developed that employs advanced physical models to simulate electron scattering in a 3D target. The software was used to simulate results for SEM signals in defect inspection and linewidth measurement, energy deposition in EBL, and electron spectra. It was found that the detection of dimensions in CD-SEM depends greatly on SEM parameters and on the type of pattern being measured. Results produced using the DLA model were compared to those using CSDA and to experimental data; DLA showed higher accuracy.

References

[1] D. C. Joy, Monte Carlo Modeling for Electron Microscopy and Microanalysis, Oxford University Press, 1995.
[2] M. Kotera, J. Vac. Sci. Technol. B19 (6) (2001) 2516.
[3] G. Han, F. Cerrina, J. Vac. Sci. Techol. B20 (6) (2002) 2666.
[4] J. R. Lowney, M. T. Postek, J. S. Villarrubia, A. E. Vladar, Scanning March (2001) 178.
[5] V. Ivin, M. Silakov, G. Babushkin, B. Lu, P. Mangat, K. Nordquist, D. Resnick, Microelectronic Engineering v.69 (2-4) (2003) 594.
[6] L. Landau, Journal of Physics, USSR v.8 (1944) 201.
[7] H. Bethe, Ann. Phys. 5(5) (1930) 325.
[8] M. Gryzinski, Phys. Rev. v.138(2A) (1965) A305.
[9] C. Moeller, Annalen der Physik v.14 (1932) 31.
[10] D. Pines, Review of Modern Physics v.28(3) (1956) 185.
[11] T. Koshikawa, R. Shimizu, J. Phys. D. Appl. Phys. v.6 (1973) 1369.
[12] M.P.Seah, W.A.Dench, Surface and Interface Analysis v.1 (1979) 2.
[13] S. Tanuma, C. J. Powell and D. R. Penn, Surf Interface Anal. v.17 (1991) 911; Surf Interface Anal. v.21 (1993) 165.
[14] R. Shimizu., T. Ikuta, K. Murata, J. Appl. Phys. v.43(10) (1972) 4233.
[15] S. Babin, S. Borisov, A. Ivanchikov, I. Ruzavin, JVST B v.6 (2006) to be published